Supplementary Information

Effects of metal doping on the methanol deep oxidation activity of the Pd/CeO_2 monolithic catalyst

Yue Li‡, Jingjing Zhang,‡ Yile Lin, Piracha Sanwal, Lulu Zhou, Gao Li* and Yongdong Chen*

Materials

All the chemicals were used as received. Sodium tetrachloropallate (99%, Aladdin), Polyvinyl pyrrolidone (99%, Sinopharm), L-ascorbic acid (99%, D&B), Cerium nitrate (99%, Aladdin), Sodium hydroxide (99%, Kelong), Bismuth nitrate (99%, Aladdin), Lanthanum nitrate (99%, Aladdin), Magnesium nitrate (99%, Aladdin), Zirconium nitrate, Acetone (99%, Kelong), Glacial acetic acid (99.5%, Kelong), Methanol (99.9%, Adamas), O_2 (99.999%, Zhengrong) N_2 (99.9%, Zhengrong).

Catalyst Characterization

Powder X-ray diffraction (XRD) patterns were recorded on a DX-2700 multifunctional diffractometer using Cu-Kα radiation of 0.15406 nm at 40 kV and 40 mA to analyze the phase structure of the samples. The XRD data was recorded in the 2θ range of 10 ~ 90°. The textural properties were measured at -196 °C on a Micromeritics ASAP2460 analyzer using nitrogen adsorption/desorption method. The specific surface areas of the samples were calculated from the adsorption curve using the Brunauer-Emmett-Teller (BET) method, and the pore volume and pore size were determined using Barrett-Joyner-Halenda (BJH) desorption theoretical model. The samples were degassed at 300 °C for 3 h under vacuum before the measurements. Transmission electron microscopy (TEM) images were recorded on a Thermo Scientific Talos F200S Transmission Electron Microscope with an accelerating voltage of 200 kV. The specimens were prepared by ultrasonic dispersion in ethanol, depositing the sample suspension droplets on a carbon-coated Cu grid, and drying in air. The Raman spectra were acquired on a Thermo Scientific Dxr2xi Raman spectrometer using an excitation laser line of 325 nm with a range of 50–2000 cm^{-1}. The X-ray photoelectron spectroscopy (XPS) measurements were carried out on a thermos scientific NEXSA spectrometer with Al-Kα radiation. All the element binding energies were referenced to the adventitious carbon (C 1s) situated at 284.8 eV. Temperature-programmed reduction by hydrogen (H_2-TPR) was conducted using an automatic multipurpose adsorption instrument TP-5076 (Xianquan Industrial and Trading Co., Ltd.). 50 mg sample was loaded into a quartz reaction tube and pretreated with N_2 (30 mL/min) at 300 °C for 1 h to remove surface impurities. After cooling down to room temperature, the sample was exposed to 5% H_2/N_2 mixture (30 mL/min) and heated to 900 °C at a rate of 10 °C/min. The effluent was analyzed using a thermal conductivity detector (TCD). After being purged with pure He at room temperature, NH_3 desorption took place in the temperature ranges of 50~800 °C at a heating rate of 10°C/min in a flow of He.

Catalytic performance measurement

The catalyst activity evaluation was carried out in a laboratory assembled multi-channel fixed-bed continuous flow reactor. The catalyst was directly loaded into the reactor, and the activity test was carried out by temperature programmed. The gas in each channel was metered into the mixer with a mass flow meter and introduced into the mixer for uniform mixing. The volume composition of the simulated gas is 200 ppm CH_3OH, 2.0 vol.% O_2, and N_2 as balance gas. The total flow rate was 1015.6 mL·min^{-1} with a GHSV (gas hourly space velocity) of 30000 h^{-1}. The reaction gas flow should be stabilized for 0.5 h before each measurement. Concentrations of CH_3OH in inlet and outlet streams were monitored online by gas chromatograph (Agilent GC 7890B), FID detector, HP-INNOWAX capillary column, concentrations of inorganic gas like CO_2 were detected by TCD detector. CH_3OH conversion were calculated according to the following formula:

$$CH_3OH\ conversion(\%) = \frac{[CH_3OH]_{inlet} - [CH_3OH]_{outlet}}{[CH_3OH]_{inlet}} \times 100\%$$

The kinetic parameters were used to evaluate the reaction rate of the catalysts. The apparent activation energy values E_a of CH_3OH were calculated by the following formula equation:

$$k = -\frac{V'}{m_{cat}} ln(1-\alpha)$$

$$k = Aexp(-\frac{E_a}{RT})$$

, where R was the universal gas constant (8.314 J·mol^{-1}·K^{-1}), α was the CH_3OH conversion (less than 20%), m_{cat} was the mass of catalyst (0.35 g), k represented the reaction rate constant (cm^3·(g·s)$^{-1}$); V' was the total gas flow rate (16.9 cm^3·s^{-1}).

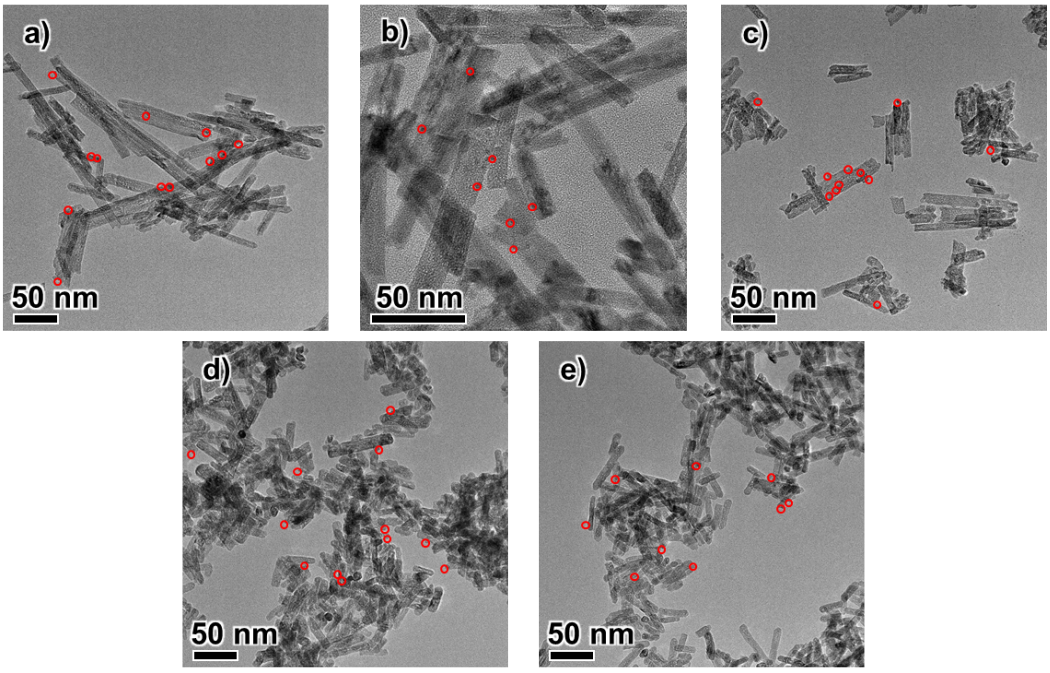

Figure S1. TEM images of Pd/CeM: (a) Pd/CeO_2, (b) Pd/CeMg, (c) Pd/CeLa, (d) Pd/CeBi and (e) Pd/CeZr.

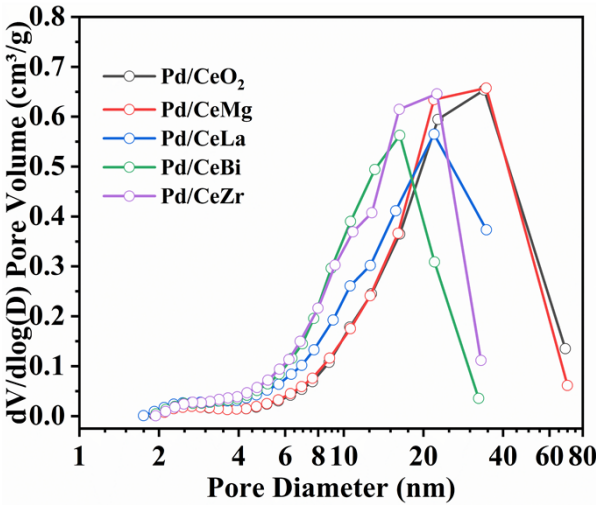

Figure S2. Pore size distribution curves of Pd/CeM catalyst.

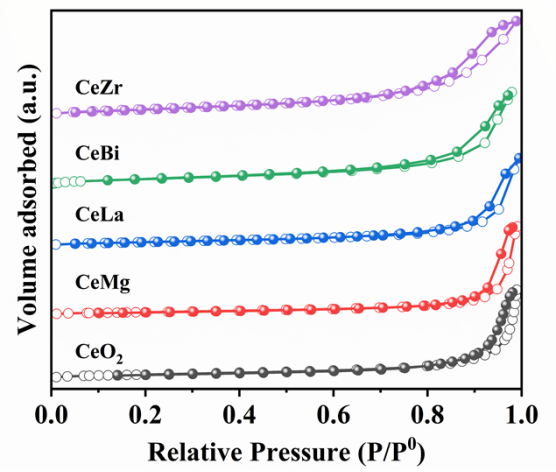

Figure S3. N_2 adsorption/desorption isotherms of CeM support.

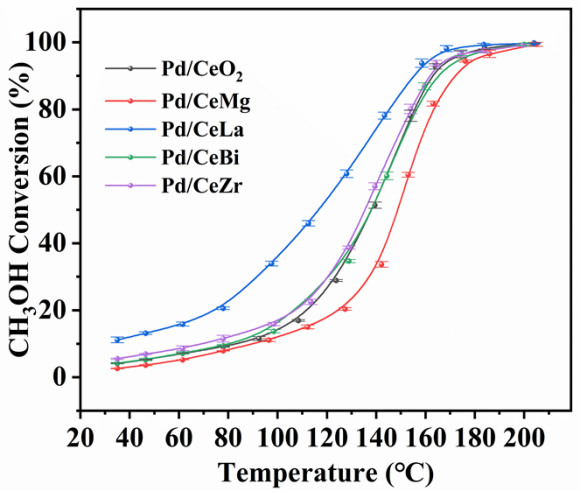

Figure S4. Catalytic performance of Pd/CeM catalysts with error bars.

Table S1. Lattice parameters of CeM and Pd/CeM (M=La, Mg, Bi, Zr).

Samples	(111) plane		Crystallite sizes (nm)[a]	Lattice parameter (nm)
	2θ (°)	d (nm)		
CeO_2	28.560	0.3123	9.7	0.5409
CeMg	28.570	0.3122	9.7	0.5407
CeLa	28.321	0.3149	8.6	0.5454
CeBi	28.460	0.3134	8.5	0.5428
CeZr	28.600	0.3119	8.6	0.5402
Pd/CeO_2	28.520	0.3127	9.5	0.5416
Pd/CeMg	28.620	0.3116	9.5	0.5397
Pd/CeLa	28.418	0.3138	8.5	0.5435
Pd/CeBi	28.361	0.3144	8.4	0.5446
Pd/CeZr	28.581	0.3121	8.6	0.5406

[a] As calculated by the Scherrer equation, based on the (111) crystal plane with the strongest diffraction intensity of ceria, and the crystallite size of the nanorod sample refers to the diameter of the nanorods.

Table S2. Structural properties of Pd/CeO_2 and Pd/CeM catalysts.

Catalysts	Pd content (wt%)[a]	BET surface (m^2/g)[b]	Pore volume (cm^3/g)	Pore size (nm)
Pd/CeO_2	0.35	90	0.25	21.8
Pd/CeMg	0.33	84	0.25	20.7
Pd/CeLa	0.34	94	0.25	14.7
Pd/CeBi	0.33	90	0.24	11.3
Pd/CeZr	0.32	101	0.29	12.8

[a] Pd content measured by ICP-AES; [b] The specific surface area was calculated by the BET method.

Table S3. The chemical state of Pd species and the relative ratios of the surface concentration of Ce^{3+} and oxygen vacancy based on XPS analysis of Pd/CeM (M=Mg, La, Bi, Zr) catalysts. $Ce^{3+}\% = Ce^{3+}/(Ce^{3+}+Ce^{4+})$; $O_V\% = O_V/(O_C+O_V+O_L)$.

Sample	Content (%)			
	PdO_x/Pd^a	$Pd^{\delta+}/Pd^a$	$Ce^{3+}\%$	$O_V\%$
Pd/CeO_2	77.4	22.6	30.5	31.2
Pd/CeMg	77.8	22.2	31.2	31.9
Pd/CeLa	63.2	36.8	33.6	38.9
Pd/CeBi	69.7	30.3	33.0	32.0
Pd/CeZr	66.8	33.2	33.4	33.5

Pd^a represent the total content of all forms of Pd species in the catalyst, $Pd^a = (PdO_x + Pd^{\delta+})$, $(0 < x \leq 1, \delta > 2)$, PdO_x and $Pd^{\delta+}$ with the signal around 335.9~336.9 eV and 337.0~338.6 eV, respectively.

Table S4. T_{50} and T_{90} of Pd/CeM catalysts in methanol oxidation reaction.

Catalyst	T_{50}/°C	T_{90}/°C	$\triangle T$/°C
Pd/CeO_2	139	163	24
Pd/CeMg	149	172	23
Pd/CeLa	118	155	37
Pd/CeBi	138	165	27
Pd/CeZr	135	162	27

Table S5 Summary of reaction conditions and catalytic activity for methanol deep oxidation over various supported catalyst.

Sample	Gas Component	T_{50} (°C)	T_{90} (°C)	by-products	Refs.
0.5%Pd/beta	1%CH_3OH, 0.15%CO, 2%O_2, N_2	145	160	HCHO	[1]
0.5%Pd/La_2O_3-Al_2O_3	1%CH_3OH, 2%O_2, N_2	187	205	—	[2]
0.1%Pt/γ-Al_2O_3	0.2%CH_3OH, 1%O_2, N_2	169	195(T_{95})	HCHO, CO	[3]
0.1%Pd/γ-Al_2O_3	0.2%CH_3OH, 1%O_2, N_2	187	239(T_{95})	HCHO, CO	[3]
6%Ag/LSM/γ-Al_2O_3	0.2%CH_3OH, 1%O_2, N_2	140	175(T_{95})	little	[3]
2.3%Ag/CeIn-NP	0.02%CH_3OH, 2%O_2, N_2	120	160	—	[4]
2%Pd-Ba/CZLA	0.02%CH_3OH, 2%O_2, CO, NO, C_3H_8, N_2	142	160	—	[5]
0.33%Pd/CeLa	0.02%CH_3OH, 2%O_2, N_2	118	155	—	this work

Table S6 The conversion of methanol oxidation under Pd/CeM catalyst as a function of reaction temperature and the mean and standard deviation of the obtained data

Catalysts	Temperature (°C)	CH_3OH Conversion (%)			Mean (%)	Standard Deviation
	35.0	4.13	4.21	4.05	4.13	0.08
	46.5	5.19	5.15	5.35	5.23	0.101
	61.5	6.99	7.25	7.15	7.13	0.13
	78.0	8.89	9.15	9.26	9.10	0.19
	92.5	12.08	11.68	10.95	11.57	0.57
Pd/CeO_2	108.5	17.16	16.68	17.01	16.95	0.25
	123.8	29.16	28.58	28.87	28.87	0.29
	139.5	50.59	52.38	51.17	51.38	0.91
	154.0	79.35	78.69	76.2	78.08	1.66
	164.0	92.86	92.01	93.59	92.82	0.79
	174.1	95.68	95.97	97.58	96.41	1.02

	184.0	97.98	99.02	98.32	98.44	0.53
	204.0	99.89	99.92	99.74	99.85	0.10
Pd/CeMg	35.0	2.54	2.60	2.72	2.62	0.09
	46.5	3.56	3.81	3.49	3.62	0.17
	61.5	5.22	5.16	5.19	5.19	0.03
	78.0	7.95	7.92	7.80	7.89	0.08
	96.5	10.89	11.65	10.82	11.12	0.46
	112.2	15.37	15.32	14.37	15.02	0.56
	127.4	20.45	19.98	20.74	20.39	0.38
	142.2	32.95	33.46	34.63	33.68	0.86
	153.0	59.89	61.26	60.32	60.49	0.70
	163.1	82.45	81.68	80.97	81.75	0.74
	176.2	94.35	94.74	94.15	94.42	0.30
	186.0	95.78	96.20	97.87	96.60	1.11
	205.0	99.56	98.75	99.95	99.42	0.61
Pd/CeLa	35.0	12.05	11.06	10.37	11.16	0.84
	46.5	12.89	13.02	13.57	13.16	0.36
	61.5	16.48	15.26	15.89	15.85	0.61
	78.0	21.03	20.34	20.43	20.60	0.38
	97.6	33.90	34.67	33.28	33.95	0.70
	112.5	45.69	46.86	45.30	45.95	0.81
	128.0	59.48	61.28	61.61	60.79	1.15
	143.4	77.65	79.36	77.41	78.14	1.06
	158.5	92.45	94.89	94.06	93.80	1.24
	168.5	99.21	97.74	97.56	98.17	0.91
	183.6	98.98	99.70	99.46	99.38	0.37
	204.0	99.56	99.89	99.62	99.69	0.18
Pd/CeBi	35.0	3.98	4.26	4.36	4.20	0.20
	46.5	5.69	5.23	4.98	5.30	0.36
	61.5	7.56	6.98	7.14	7.20	0.30
	78.0	9.02	9.56	9.59	9.39	0.32
	98.4	13.24	14.16	13.79	13.73	0.46
	128.9	35.16	34.68	34.20	34.68	0.48
	144.3	58.96	60.20	61.23	60.13	1.14
	159.6	87.28	85.73	87.69	86.90	1.03

	174.4	96.02	97.23	97.54	96.93	0.80
	190.0	97.32	99.36	98.43	98.37	1.02
	204.6	99.58	98.99	99.63	99.40	0.36
Pd/CeZr	35.0	5.64	5.29	5.56	5.52	0.20
	46.5	6.79	6.87	7.10	6.92	0.16
	61.5	7.98	9.41	8.56	8.65	0.72
	78.0	12.65	10.96	10.89	11.50	1.00
	98.5	16.36	16.01	15.33	15.90	0.52
	113.5	21.69	22.59	23.28	22.52	0.80
	129.0	38.39	38.24	38.56	38.73	0.45
	139.5	55.98	58.02	57.09	57.03	1.02
	154.0	81.23	80.65	78.57	80.15	1.40
	164.0	92.89	94.56	94.01	93.82	0.85
	174.0	97.36	97.02	95.63	96.67	0.92
	184.0	96.79	97.72	98.05	97.52	0.65
	194.2	97.89	98.56	99.50	98.65	0.81
	204.5	98.98	99.56	98.91	99.15	0.37

References

[1] X. Zhang, X. Chen, X. Liu and M. Guo, Effects of Support on Performance of Methanol Oxidation over Palladium-Only Catalysts, *Water Air Soil. Poll.*, 2020, **231**, 1-12.

[2] X. Zhang, J. Zhan, J. Yu, J. Liu, J. Liu and Y. Yang, Effects of Modified-Alumina on Performance of Methanol Oxidation over Only-Palladium Catalyst, *Journal of the Chinese Society of Rare Earths*, 2018, **36**, 42-52

[3] W. Wang, H. Zhang, G. Lin and Z. Xiong. Study of $Ag/La_{0.6}Sr_{0.4}MnO_3$ catalysts for complete oxidation of methanol and ethanol at low concentrations, *Appl. Catal. B Environ*, 2000, **24**, 219-232.

[4] L. Zhang, Y. Li, C. Liang, Y. Xiao, Y. Gong, J. Deng and Y. Chen, Tailoring metal-support interaction for preferential methanol oxidation over $Ag/Ce_{0.90}In_{0.10}O_{\delta}$ nanocatalysts with different morphology, *Mol Catal.*, 2024, **565**, 114302.

[5] X. Zhang, M. Zhang, C. Xu, J. Wang and Y. Chen, Effect of BaO on catalytic performance of Pd-based catalysts for purification of gasoline-methanol exhaust, *J. Rare Earth*, 2014, **32**,603-609.